



Article

Composite Ceramics Based on Pastes Including Tricalcium Phosphate and an Aqueous Solution of Sodium Silicate

Maksim Kaimonov ^{1,*}, Tatiana Safronova ^{1,2}, Tatiana Shatalova ^{1,2}, Yaroslav Filippov ^{1,3}, Irina Tikhomirova ⁴ and Yulia Lukina ^{5,6}

- ¹ Department of Materials Science, Lomonosov Moscow State University, Building, 73, Leninskie Gory, 1, 119991 Moscow, Russia
 - ² Department of Chemistry, Lomonosov Moscow State University, Building, 3, Leninskie Gory, 1, 119991 Moscow, Russia
 - ³ Research Institute of Mechanics, Lomonosov Moscow State University, Michurinsky Pr., 1, 119192 Moscow, Russia
 - ⁴ Department of General Technology of Silicates, Mendeleev University of Chemical Technology, Building, 1, Geroyev Panfilovtsev, 20, 125480 Moscow, Russia
 - ⁵ Priorov National Medical Research Center of Traumatology and Orthopedics, Priorova, 10, 127299 Moscow, Russia
 - ⁶ Department of Engineering Design of Technological Equipment, Mendeleev University of Chemical Technology, Miusskaya, 9, 125047 Moscow, Russia
- * Correspondence: kaimonovmr@my.msu.ru

Abstract: Preceramic samples were prepared from pastes based on the aqueous solution of sodium silicate and tricalcium phosphate with a given molar ratio of $(\text{Na}_2\text{O} \cdot 2,87\text{SiO}_2)_{\text{aq}} / \text{Ca}_3(\text{PO}_4)_2 = 1:3$ after drying at 24 °C and then 60 °C for 24 h. It established the dependence of the plastic strength of these pastes on both time and temperature and the possibility of using them for extrusion 3D printing. The phase composition of ceramic was represented by unreacted β -TCP ($\beta\text{-Ca}_3(\text{PO}_4)_2$) and β -rhenanite ($\beta\text{-NaCaPO}_4$) after heat treatment at 500 °C. Further, an increase in temperature up to 700 °C led to the appearing phase of silicon dioxide (SiO_2) and up to 900 °C, of sodium calcium phosphate ($\text{Na}_3\text{Ca}_6(\text{PO}_4)_5$). After heat-treatment at 1100 °C, ceramic samples consisted of the β -TCP ($\beta\text{-Ca}_3(\text{PO}_4)_2$), sodium calcium phosphate ($\text{Na}_3\text{Ca}_6(\text{PO}_4)_5$), silicon dioxide (SiO_2) and β -wollastonite ($\beta\text{-CaSiO}_3$). The bending and compressive strength of the ceramics rose with increasing temperature from ≈ 6.8 MPa and ≈ 31.1 MPa at 500 °C to ≈ 10.6 MPa and ≈ 43.5 MPa at 1100 °C. The obtained composite ceramics consisted of biocompatible phases that are widely studied in the literature and may be used as a biomaterial for the treatment of bone tissue defects.

Keywords: tricalcium phosphate; aqueous solution of sodium silicate; paste; preceramic sample; ceramic; composite



Citation: Kaimonov, M.; Safronova, T.; Shatalova, T.; Filippov, Y.; Tikhomirova, I.; Lukina, Y.

Composite Ceramics Based on Pastes Including Tricalcium Phosphate and an Aqueous Solution of Sodium Silicate. *J. Compos. Sci.* **2022**, *6*, 267. <https://doi.org/10.3390/jcs6090267>

Academic Editor:
Francesco Tornabene

Received: 31 July 2022

Accepted: 2 September 2022

Published: 11 September 2022

Publisher's Note: MDPI stays neutral with regard to jurisdictional claims in published maps and institutional affiliations.



Copyright: © 2022 by the authors. Licensee MDPI, Basel, Switzerland. This article is an open access article distributed under the terms and conditions of the Creative Commons Attribution (CC BY) license (<https://creativecommons.org/licenses/by/4.0/>).

1. Introduction

The experience of researchers reflected in the scientific literature [1–4] indicates the need to expand the phase structure of materials for bone implants based on calcium phosphates. Bioresorbable phases should be present in composition along with hydroxyapatite (HA) and tricalcium phosphate (TCP), or instead of them, which have a lower molar ratio of Ca/P for a successful implementation of the regenerative treatment method of bone defects [5–8]. Sodium calcium phosphates are also suitable for that purpose, such as β -rhenanite NaCaPO_4 and Na-substituted TCP $\text{Ca}_{10}\text{Na}(\text{PO}_4)_7$ (which can also be called double calcium phosphates) or the $\text{Na}_3\text{Ca}_6(\text{PO}_4)_5$ phase, because these phases increase the bioactivity of ceramics [9–12]. Double calcium phosphates have a higher solubility relative to TCP and, accordingly, HA, due to the replacement of the Ca^{2+} ion by an ion with a larger radius and (or) a lower charge. Usually, double calcium phosphates are obtained at high

temperatures (above 500 °C) by the interaction of calcium phosphates and an alkali metal compound [13].

On the other side, the calcium phosphate material can be supplemented with a more osteoinductive phase containing silica in its composition [1,14]. The most common composites are calcium phosphate (HAP and (or) TCP) with Bioglass 45S5 [12,15,16], in which $\text{Na}_3\text{Ca}_6(\text{PO}_4)_5$ is formed as the base or secondary phase. Materials containing $\text{Na}_3\text{Ca}_6(\text{PO}_4)_5$ show promising trends in both in vitro and in vivo tests in those works. $\text{Na}_3\text{Ca}_6(\text{PO}_4)_5$ belongs to the $\text{NaCaPO}_4\text{—Ca}_3(\text{PO}_4)_2$ [17] system, and in [18], it was established in the high-temperature range (650–1200 °C) that the $\beta\text{-NaCaPO}_4$ phase transformed into $\alpha\text{-NaCaPO}_4$, which then dissolved in $\beta\text{-TCP}$ and formed a $\text{Na}_3\text{Ca}_6(\text{PO}_4)_5$ compound. Then, $\text{Na}_3\text{Ca}_6(\text{PO}_4)_5$ and $\beta\text{-TCP}$ changed to a Na–Ca–P–O glass phase at elevated temperature. During the cooling, $\text{Na}_3\text{Ca}_6(\text{PO}_4)_5$ and $\beta\text{-NaCaPO}_4$ formed again. Similar results were observed in [19] but at higher temperatures (900–1700 °C). It is important to note that in [17,20], the $\text{Na}_2\text{Ca}_5(\text{PO}_4)_4$ phase was shown, and in [20], the authors suggested that the phosphate referred to as $\text{Na}_3\text{Ca}_6(\text{PO}_4)_5$ did not exist and was actually $\text{Na}_2\text{Ca}_5(\text{PO}_4)_4$, because the $\text{Na}_3\text{Ca}_6(\text{PO}_4)_5$ compound was previously formulated without taking into account the volatilization of Na_2O at high temperature. However, according to the X-ray diffraction analyses, only $\text{Na}_3\text{Ca}_6(\text{PO}_4)_5$ leads to a pure compound in agreement with the PDF [20].

In [21], the authors found that when they implanted composites of the composition $\beta\text{-NaCaPO}_4$ and $\alpha\text{-cristobalite}$ into a bone defect, an excellent osteoconductive effect was observed. The bone defects were filled with bone tissue after 3 weeks incorporating minimal residues of graft material. These results indicate that the Si-rich calcium phosphate ceramic containing high silica concentrations not only has a measurable stimulatory effect on bone cell function but also resorbs in harmony with the rate of new bone formation. It is due to the physicochemical properties of its mineral constituents as $\beta\text{-NaCaPO}_4$ contains Na ions weakening the bond between Ca^{2+} and the PO_4^{3-} in the crystal surface and acts as a weak interphase for $\alpha\text{-cristobalite}$. Hence, all that provides an easy path for structure debonding, which facilitates silica dissolution and leads to rapid bone regeneration. The authors note the architecture of the remodeled cortical bone and marrow resembles that of normal healthy bone. In [22], the authors found that the neonatal rat calvarial osteoblasts attached to the composite consisting of $\beta\text{-NaCaPO}_4$ and $\alpha\text{-cristobalite}$ expressed considerably higher mRNA levels of collagen-I, osteocalcin and osteopontin genes compared to those expressed by cells attached onto the surface of other ceramic samples. The stimulation of gene expression of bone proteins by this composite can explain the expedited and abundant bone formation observed in defects grafted with such material.

In the tissue engineering design, a way of treatment suggests the possibility of using bioactive scaffolds to eliminate bone tissue defects. These scaffolds can be obtained from bioactive materials using additive technologies, which, in turn, allow the preparation of a matrix individually for each person or animal to target reconstructing a bone tissue defect.

Extrusion 3D printing was one of the first used technologies for the layer-by-layer reconstruction of three-dimensional objects. The application of extrusion 3D printing made it possible to study the pore geometry, structure gradient, permeability and mechanical properties of ceramic and bioglass scaffolds of various architectures [23–25]. Hexagonal pores have been found to give the highest compressive strength at 70% porosity, which is within the range of 100–150 MPa for cortical bone [26]. At the same time, this method has several limitations: it applies only to viscous fluid systems, it has a low printing speed, it requires spinnerets with different diameters to adjust the thickness of the extruded material and the spinnerets can be clogged, plus stepped edges are observed during 3D printing. However, extrusion 3D printing has wide use, and special attention is paid to the extrudable material, the rheological properties of which change with a change in the phase composition.

In the general case, the extruded material is presented as constituting highly concentrated suspensions (pastes), which contain a binder and a dispersed filler in their

composition. In such suspensions, forces act between the particles, leading to the formation of structures.

Several requirements are imposed on the pastes:

1. The paste should be homogeneous and free of air bubbles;
2. It should possess a large volume fraction of the filler;
3. It should possess sedimentation resistance;
4. It should possess a fluidity suitable for extrusion;
5. During extrusion, delamination should not be observed;
6. It should maintain its shape after printing.

These criteria make it possible to achieve a high-resolution and quality extrusion printing of biocompatible materials.

Water [4], polymer or organic solvent [25,27] and hydrogels [28] were considered as binding components for pastes. In addition to the above binders, aqueous solutions of sodium silicate ($\text{Na}_2\text{O}\cdot n\text{SiO}_2$) can be dealt with for the extrusion printing of biocompatible materials, which are environmentally friendly, nontoxic and cheap [29]. Sodium silicate can form a hydroxyapatite layer on its surface in SBF tests [30], and it was used to obtain silicon-substituted hydroxyapatite (Si-HA) materials [31].

Thus, the purpose of the current work was to obtain composite ceramics containing sodium calcium phosphates and silica compounds based on synthetic tricalcium phosphate and an aqueous solution of sodium silicate. We considered the possibility of using pastes containing tricalcium phosphate and an aqueous solution of sodium silicate as an extrusion material for obtaining scaffolds by extrusion 3D printing to eliminate bone tissue defects.

2. Materials and Methods

2.1. Samples Preparation

Pastes were based on tricalcium phosphate $\text{Ca}_3(\text{PO}_4)_2$ (CAS No. 7758-87-4, purum. p.a. $\geq 96\%$, Sigma-Aldrich CHEMIE GmbH, 21218, Lot BCBK8832V, Steinheim, Germany) and the aqueous solution of sodium silicate $(\text{Na}_2\text{O}\cdot 2,87\text{SiO}_2)_{\text{aq}}$ (GOST 13078-81, JSC "Salavatsteklo", Salavat, Russian Federation).

The method of preparing pastes, preceramic samples formation and obtaining composite ceramic samples was described in more detail in previous work [32].

Briefly, the initial reagents were taken in the molar ratio $(\text{Na}_2\text{O}\cdot 2,87\text{SiO}_2)_{\text{aq}}/\text{Ca}_3(\text{PO}_4)_2 = 1:3$ ($\text{SS}_{\text{aq}}/\text{TCP}$) for obtaining plastic molding mass. Then, preceramic samples in sizes $30\text{ mm} \times 10\text{ mm} \times 10\text{ mm}$ were molded from pastes, and after that, prepared preceramic materials were fired in the air in a furnace to obtain ceramics. The temperature range was $500\text{--}1100\text{ }^\circ\text{C}$, a heating rate of $5\text{ }^\circ\text{C}/\text{min}$, an exposure time of 2 h, and cooling in the furnace.

In the current work, together with preparing preceramic samples in size $30\text{ mm} \times 10\text{ mm} \times 10\text{ mm}$, an attempt to obtain simple three-dimensional geometric shapes from prepared pastes based on TCP and SS_{aq} using layer-by-layer extrusion hand molding was considered. A disposable syringe of 10 mL with a spinneret of 0.75 mm in diameter was used for the extrusion of 3D shapes.

2.2. Characterization

2.2.1. Pastes Plastic Strength Determination

The plastic strength was measured by the conical plastometer method, which consists in determining the kinetics of immersion (penetration depth) of the cone into the studied disperse system under the action of a constant load F . When the cone is immersed in the material under study, stresses arise in it. That prevents the penetration of the cone into the material. A lever-type conical Rebinder's plastometer was used in the work (the plastometer was developed at the Faculty of Technology of Inorganic Substances and High-Temperature Materials of the Mendeleev University of Chemical Technology, Moscow, the Soviet Union).

The plastic strength was determined by the formula:

$$R = \frac{L}{l} * K * \frac{F}{h^2}, \quad (1)$$

where R is the plastic strength, in Pa;

L and l are plastometer arms, in cm;

K is a dimensionless coefficient depending on the angle at the cone apex;

F is a load, in g;

h is an immersion depth of the cone, in mm.

The cone constant K is determined by the formula:

$$K = \frac{\cos^2\left(\frac{\alpha}{2}\right) * \text{ctg}\left(\frac{\alpha}{2}\right)}{\pi}, \quad (2)$$

where α is the angle at the cone apex.

At $\alpha = 60^\circ$, $K = 0.413$.

The measurements were carried out at room temperature, 60°C and 100°C .

2.2.2. Determination of the Strength Properties

The strength characteristics of the obtained ceramics after heat treatment of the pre-ceramic samples of size $30\text{ mm} \times 10\text{ mm} \times 10\text{ mm}$ molded from pastes based on tricalcium phosphate $\text{Ca}_3(\text{PO}_4)_2$ and the aqueous solution of sodium silicate $(\text{Na}_2\text{O} \cdot 2,87\text{SiO}_2)_{\text{aq}}$ in the molar ratio $(\text{Na}_2\text{O} \cdot 2,87\text{SiO}_2)_{\text{aq}} / \text{Ca}_3(\text{PO}_4)_2 = 1:3$ were determined using a universal testing machine of the FM PW 500 (VEB Thüringer Industrierwerk, Rauenstein, Germany) and PGM-100MG4 (OOO "Special Design Bureau Stroypribor", Chelyabinsk, Russian Federation).

2.2.3. Structural Characterization

The diffractometer Rigaku D/Max-2500 with a rotating anode (Tokyo, Japan), a 2θ angle range of $2\text{--}70^\circ$ with a step of 0.02° , a rate of spectrum registration of $5^\circ/\text{min}$ and a $\text{CuK}\alpha$ radiation ($\lambda = 1.5406\text{ \AA}$) was used for the investigation samples by X-ray powder diffraction. The phases were determined using the ICDD PDF-2 database [33].

The electron microscope LEO SUPRA 50VP (Carl Zeiss, Jena, Germany; auto-emission source) with an accelerating voltage of 20 kV (SE2 detector) was used for the investigation samples by scanning electron microscopy (SEM). The samples were precoated with a layer of chromium (up to 20 nm).

The particle size distribution of a tricalcium phosphate $\text{Ca}_3(\text{PO}_4)_2$ (CAS No. 7758-87-4, purum. p.a. $\geq 96\%$, Sigma-Aldrich CHEMIE GmbH, 21218, Lot BCBK8832V, Steinheim, Germany) was investigated by an ANALYSETTE-22 MicroTec plus laser particle sizer (Fritsch GMBH, Idar-Oberstein, Germany).

2.2.4. Thermogravimetric and Mass Spectrometric Analysis

The NETZSCH STA 409 PC Luxx simultaneous thermal analyzer (NETZSCH, Selb, Germany) with a heating rate of $10^\circ\text{C}/\text{min}$ and an air atmosphere was used for the investigation of preceramic samples by thermal analysis (mass of sample—10 mg, temperature range— $40\text{--}1000^\circ\text{C}$). The quadrupole mass spectrometer QMS 403C Aëolos (NETZSCH, Selb, Germany) combined with a NETZSCH STA 409 PC Luxx thermal analyzer was used to determine the composition of the gas phase formed upon decomposition of the samples. The mass spectrum (MS) was recorded for an m/Z value of 18 (H_2O).

3. Results and Discussion

3.1. Pastes Characterization

Following the dependence of plastic strength on time (Figure 1), the plastic strength values were low in the first minutes after mixing the synthetic tricalcium phosphate powder

with an aqueous solution of sodium silicate. A rise in both time and temperature led to an increase in the values of the plastic strength. It was associated with the hardening of the compositions.

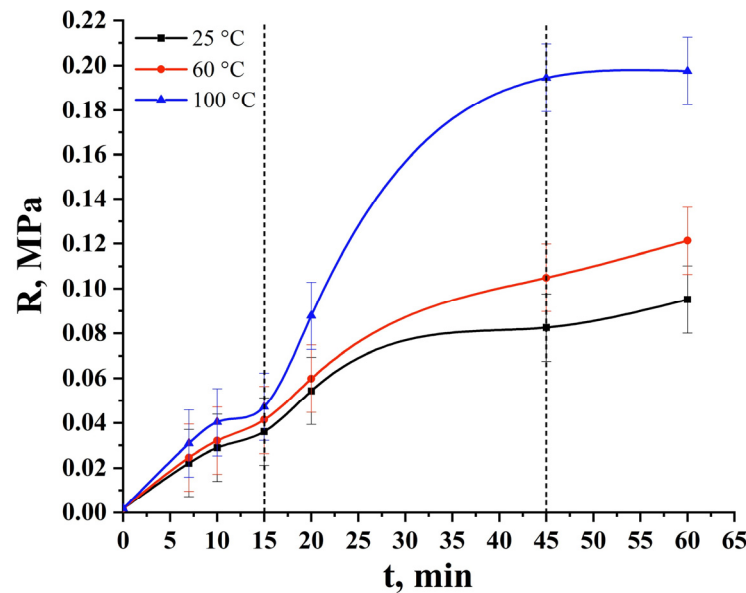


Figure 1. Dependence of plastic strength on time for compositions based on synthetic tricalcium phosphate $\text{Ca}_3(\text{PO}_4)_2$ and the aqueous solution of sodium silicate $(\text{Na}_2\text{O}\cdot 2,87\text{SiO}_2)_{\text{aq}}$.

The hardening process of the materials began at the paste surface–air interface. Figure 1 illustrates a gradual hardening of the composites, which can conditionally be divided into the following stages: The first stage in the time range of 0–15 min was characterized by the beginning of the hardening of the composites. A thin crust appeared on the surface of the samples. The second stage in the time range of 15–45 min was characterized by a further hardening deep into the composites. The crust became larger. The third (from 45 min) and subsequent stages were characterized by a further hardening of the composites until they were completely solidified.

The effect of temperature on the hardening time was observed immediately at the 1st stage. As a result, the plastic strength values were $R_{25\text{ °C}} \approx 0.036$ MPa, $R_{60\text{ °C}} \approx 0.041$ MPa and $R_{100\text{ °C}} \approx 0.047$ MPa by 15 min. The hardening process was completed in 45 min for samples at 100 °C straightway in the second stage, because the values of the plastic strength reached a plateau. The plastic strength value was $R_{100\text{ °C}} \approx 0.2$ MPa. At the same time, the plastic strength values for the composites at 25 °C and 60 °C by 45 min were, respectively, $R_{25\text{ °C}} \approx 0.08$ MPa and $R_{60\text{ °C}} \approx 0.1$ MPa. These composites would also gradually harden with a further increase in time. It is expected that the plastic strength value for solidified composites at 25 °C and 60 °C may be comparable to composites at 100 °C and reach the values of ≈ 0.2 MPa.

Thus, the formed samples did not solidify in a silicone mold after exposure to the air for 24 h at room temperature because the hardening process began at the paste surface–air interface, forming a crust. Hence, samples required demolding followed by a moderate heat treatment to prevent the appearance of defects due to internal stresses or intensive water evaporation. The content of retained water in the sample depends on the temperature and humidity of the air [34]. If the air humidity increases, the composite will exhibit hygroscopicity. In the current work, the temperature of 60 °C was chosen for the heat treatment of the demolded samples, because for 24 h at that temperature, a solidified state without visible defects occurred. The linear shrinkage of such composites was no more than 2%. A solidified state was observed when the water content in SS_{aq} and, accordingly, in the samples, decreased to 20–30 wt.% [34]. That led to the formation of preceramic samples.

Highly concentrated suspensions (pastes) based on synthetic TCP powder and SS_{aq} showed excellent molding properties with shape retention. In Figure 2, the samples of preceramic blanks obtained by plastic molding (a) and layer-by-layer extrusion hand molding (b) are shown.

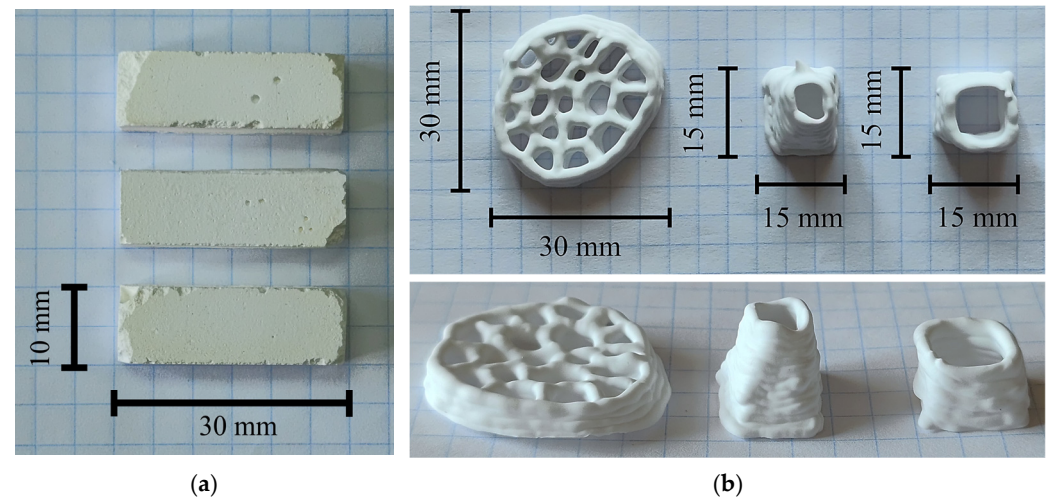


Figure 2. Samples formed by plastic molding from appropriate molds of size 30 mm × 10 mm × 10 mm (a). Samples formed by layer-by-layer extrusion hand molding (b).

A good adhesion and cohesion between the layers of the extruded material were observed in the samples obtained using layer-by-layer extrusion hand molding that complied with the requirements for this type of printing. A disposable syringe of 10 mL with a spinneret of 0.75 mm in diameter was used for the extrusion of 3D shapes. These samples indicated the possibility of using pastes based on TCP and SS_{aq} for layer-by-layer extrusion molding of both simple 3D geometric shapes and for creating an implant of a given ceramic skeleton architecture using extrusion 3D printing.

However, it should be noted that the printing process must be carried out at the first stage of hardening, while the extruded material has not had time to gain its initial strength. A time equal to 15 min may not be sufficient for using pastes directly in extrusion 3D printing, despite excellent performance in layer-by-layer extrusion hand molding. For extrusion 3D printing, the following should be taken into account: the main printing parameters (the feed rate of the mixture, the speed of the printing unit and the diameter of the spinneret) and the characteristics of the extruded material by itself (homogeneity, sedimentation resistance, viscosity and setting time). The parameters described above should be selected individually for each composition. When required, a compound may be modified by hardeners, hardening retarders, surfactants and so on.

3.2. Characterization of the Preceramic Samples

According to the XRD data (Figure 3) and the SEM data (Figure 4a,b), an interaction did not occur between TCP and SS_{aq} after mixing the initial reagents, molding the pastes into a silicon mold, solidification and drying them for 24 h both at room temperature and at 60 °C. Nevertheless, the applied techniques (XRD, SEM) did not allow us to conclude anything about surface reactions between TCP and SS_{aq} , so it should be investigated more closely in future work.

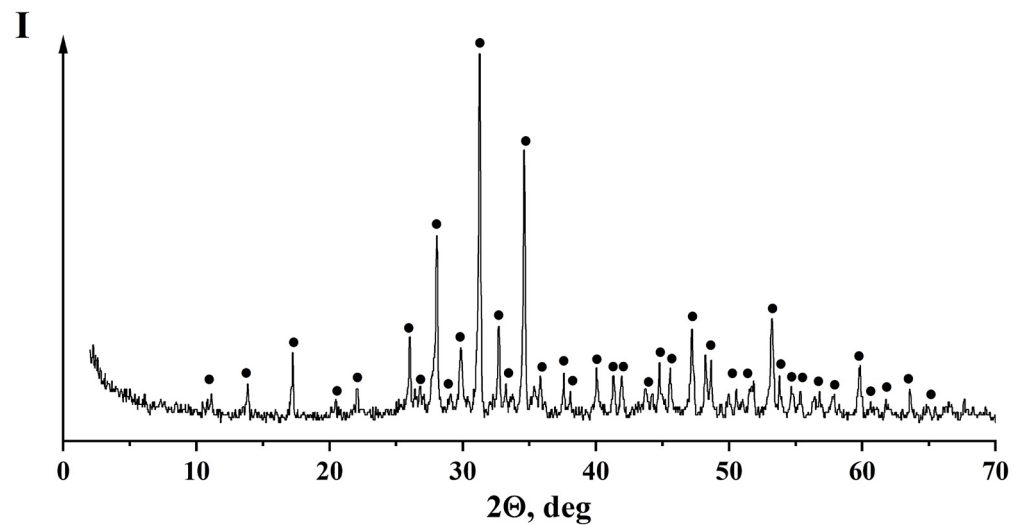
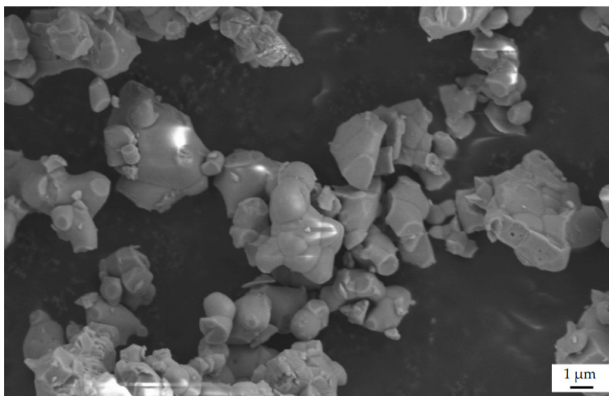
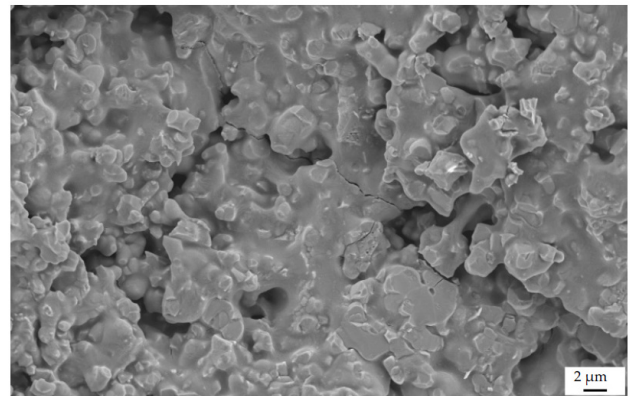


Figure 3. The X-ray diffraction pattern of the preceramic samples based on pastes included tricalcium phosphate $\text{Ca}_3(\text{PO}_4)_2$ and the aqueous solution of sodium silicate $(\text{Na}_2\text{O}\cdot 2,87\text{SiO}_2)_{\text{aq}}$; ●— $\text{Ca}_3(\text{PO}_4)_2$ (PDF card 9–169).



(a)



(b)

Figure 4. SEM micrographs of the synthetic tricalcium phosphate powder before (a) and after mixing with the aqueous solution of sodium silicate $(\text{Na}_2\text{O}\cdot 2,87\text{SiO}_2)_{\text{aq}}$ and drying at 60 °C for 24 h (b).

Figure 5 shows the particle size distribution of synthetic TCP powder. Following the data obtained in previous work [32], calcium phosphate powder particles were bound to each other by amorphous hydrated sodium silicate.

The thermal analysis (TA) and the mass spectrometry data (MS) of the samples based on TCP and SS_{aq} after drying in the air for 24 h at room temperature are shown in Figure 6 (black and grey lines, respectively). According to the TA, the total mass loss of the sample was 8% when heated up to 1000 °C. In the mass spectrum curve for $m/Z = 18$ (H_2O), there were two peaks, the first peak at 110 °C and the second at 320 °C, which correspond to the loss of physically and chemically bound water, respectively. According to Figure 7, an amorphous hydrated sodium silicate was formed after heat treatment at 100 °C. Water is removed from hydrated sodium silicate up to 600 °C, following literature data [34], and it depends on silicate modulus. The mass loss is close to a plateau above 400 °C (Figure 6), so at that moment, when the water is almost completely removed [35], polymerization processes begin in pure sodium silicate with the formation of a silicon–oxygen structure with covalent–ionic bonds [35]. The modifier cations (Na^+) form Coulomb bonds with the framework. Nevertheless, as was suggested in previous work [32], these processes described above can also occur in the sodium silicate–calcium phosphate filler system.

However, simultaneously with these processes, chemical interactions will also proceed between TCP and SS_{aq} with the formation of new phases.

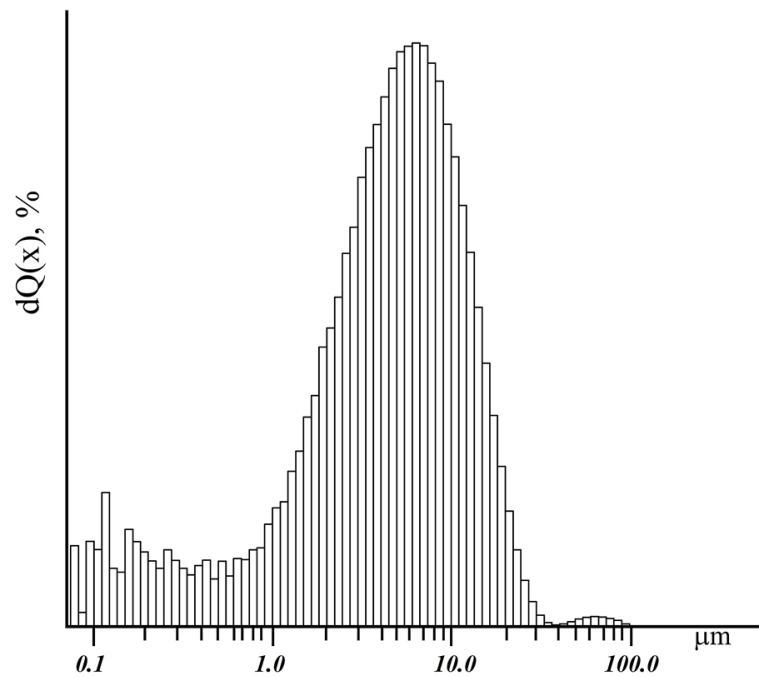


Figure 5. Particle size distribution of commercial tricalcium phosphate (Sigma-Aldrich).

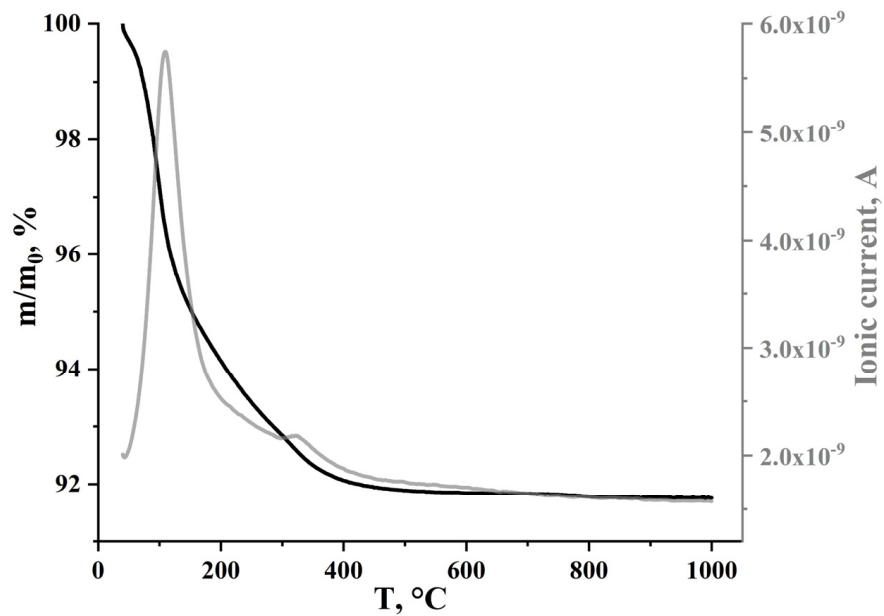


Figure 6. The results of thermal analysis (in black) and mass spectrum for evolving gas with $m/Z = 18$ (in grey) of the preceramic samples obtained from pastes after their air drying at room temperature.

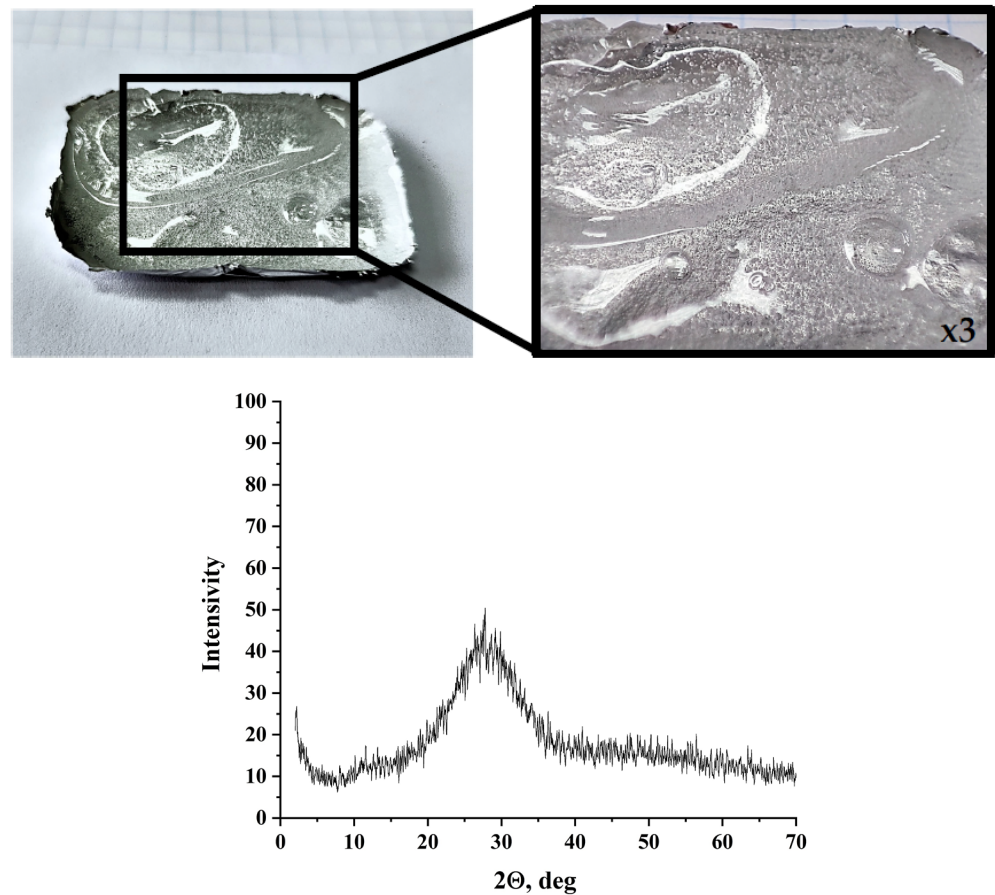


Figure 7. Appearance and XRD data of the aqueous solution of sodium silicate ($\text{Na}_2\text{O}\cdot 2,87\text{SiO}_2$)_{aq} after heat treatment at 100 °C with exposure of 24 h.

3.3. Characterization of the Ceramic Samples

The X-ray diffraction data (Figure 8) show that the phase compositions of the ceramics after heat-treatment at 500 °C consisted of β -TCP ($\beta\text{-Ca}_3(\text{PO}_4)_2$, PDF card 9–169) and β -rhenanite ($\beta\text{-NaCaPO}_4$, PDF card 29–1193). Further, an increase in temperature up to 700 °C led to the appearing phase of silicon dioxide (SiO_2 , PDF card 29–85) and up to 900 °C, of sodium calcium phosphate ($\text{Na}_3\text{Ca}_6(\text{PO}_4)_5$, PDF card 11–236). After the heat treatment at 1100 °C, ceramic samples consisted of the β -TCP ($\beta\text{-Ca}_3(\text{PO}_4)_2$, PDF card 9–169), sodium calcium phosphate ($\text{Na}_3\text{Ca}_6(\text{PO}_4)_5$, PDF card 11–236), silicon dioxide (SiO_2 , PDF card 29–85) and β -wollastonite ($\beta\text{-CaSiO}_3$, PDF card 27–88). The phase compositions of preceramic and ceramic samples are shown in Table 1.

Table 1. Phase transformation of composition into preceramic and ceramic samples after heat treatment.

Preceramic	500 °C	700 °C	900 °C	1100 °C
$\beta\text{-Ca}_3(\text{PO}_4)_2$	$\beta\text{-Ca}_3(\text{PO}_4)_2$	$\beta\text{-Ca}_3(\text{PO}_4)_2$	$\beta\text{-Ca}_3(\text{PO}_4)_2$	$\beta\text{-Ca}_3(\text{PO}_4)_2$
Nonidentified phase of hydrated $\text{Na}_2\text{O}\cdot 2,87\text{SiO}_2$	$\beta\text{-NaCaPO}_4$	$\beta\text{-NaCaPO}_4$	$\beta\text{-NaCaPO}_4$	$\text{Na}_3\text{Ca}_6(\text{PO}_4)_5$
		SiO_2	$\text{Na}_3\text{Ca}_6(\text{PO}_4)_5$	$\beta\text{-CaSiO}_3$
			SiO_2	SiO_2

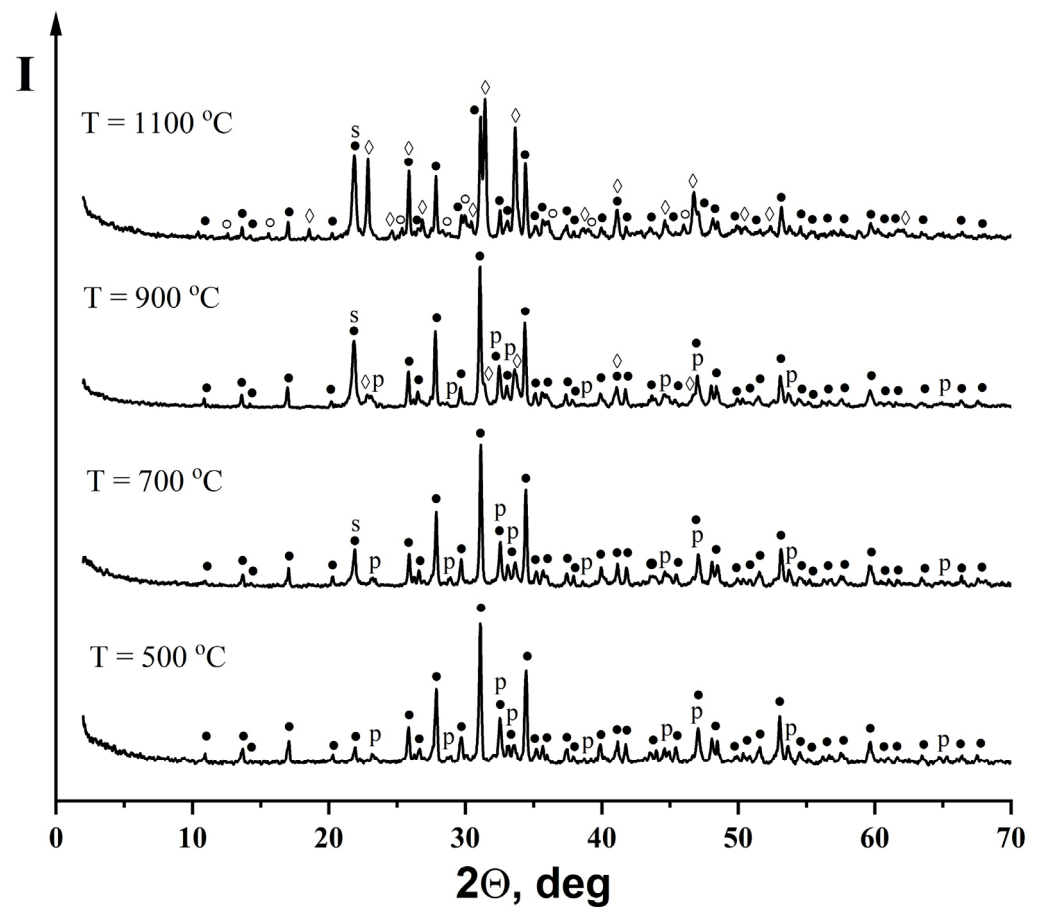


Figure 8. XRD patterns of the ceramic samples obtained from preceramic samples based on the tricalcium phosphate powder $\text{Ca}_3(\text{PO}_4)_2$ and the aqueous solution of sodium silicate $(\text{Na}_2\text{O} \cdot 2,87\text{SiO}_2)_{\text{aq}}$ after heat treatment at 500, 700, 900 and 1100 °C: ●— $\beta\text{-Ca}_3(\text{PO}_4)_2$, PDF card 9–169; ■— $\beta\text{-NaCaPO}_4$, PDF card 29–1193; ◇— $\text{Na}_3\text{Ca}_6(\text{PO}_4)_5$, PDF card 11–236; ○— $\beta\text{-CaSiO}_3$, PDF card 27–88; ■— SiO_2 , PDF card 29–85.

In the $\text{SS}_{\text{aq}}/\text{TCP}$ samples with a molar ratio $(\text{Na}_2\text{O} \cdot 2,87\text{SiO}_2)_{\text{aq}}/\text{Ca}_3(\text{PO}_4)_2 = 1:3$, the formation of a biocompatible double calcium phosphate phase of β -rhenanite ($\beta\text{-NaCaPO}_4$) can be observed at 500 °C. It should be noted that the interaction of sodium silicate with tricalcium phosphate can also form the Na-substituted TCP phase ($\text{NaCa}_{10}(\text{PO}_4)_7$). The lattice parameters of pure $\text{Ca}_3(\text{PO}_4)_2$ are $a = 10.429 \text{ \AA}$ and $c = 37.38 \text{ \AA}$ [36], and for $\text{NaCa}_{10}(\text{PO}_4)_7$, they are $a = 10.4391(1) \text{ \AA}$ and $c = 37.310(1) \text{ \AA}$ [37], which makes the determination of the presence of the Na-substituted TCP in the composition by the XRD method challenging. The determination of $\text{NaCa}_{10}(\text{PO}_4)_7$ by the EDX method can also be a challenge due to the presence of a $\beta\text{-NaCaPO}_4$ phase in the composition. Double phosphates are usually obtained at high temperatures (from 500 °C) [9–11] by the interaction of calcium phosphates with alkali metal compounds. In this case, sodium silicate acted as an alkali metal compound that interacted with tricalcium phosphate with increasing temperature, forming double calcium phosphates. It is also noted in [11] that double calcium phosphate phases are most frequently used to produce resorbable inorganic composites for regenerative bone tissue defect repairing methods. Nevertheless, it can be assumed that, since sodium silicate was deficient compared to TCP, it was not enough to obtain two phases of double calcium phosphate at once: $\beta\text{-NaCaPO}_4$ and $\text{NaCa}_{10}(\text{PO}_4)_7$. Thus, as a result of the heat treatment at 500 °C and 700 °C by the interaction of sodium silicate and TCP, only the β -rhenanite ($\beta\text{-NaCaPO}_4$) phase was formed, which then participated in a chemical reaction with unreacted TCP. This interaction led to the $\text{Na}_3\text{Ca}_6(\text{PO}_4)_5$ phase development with increasing temperatures up to 900 °C and 1100 °C.

The silicon dioxide phase began to form after heat treatment at 700 °C following XRD data, and it rose at a further increasing temperatures. Silicon dioxide is a biocompatible inorganic material [38–40] widely used in medicine, which in the human body can be subjected to both chemical and biological effects [41], demonstrating various behaviors. For example, silica gel formed in the presence of enzymes exhibits the properties of a biocatalyst [40].

The phase of $\text{Na}_3\text{Ca}_6(\text{PO}_4)_5$ began to form after 900 °C in a small amount, and it was one of the main phases at 1100 °C. This phase belongs to the $\text{NaCaPO}_4\text{--Ca}_3(\text{PO}_4)_2$ [17] system, and it was obtained in [12] upon mixing 75 wt.% hydroxyapatite with 25 wt.% Bioglass 45S5. The composition with the $\text{Na}_3\text{Ca}_6(\text{PO}_4)_5$ phase in a silicate matrix caused the highest level of mineralization on the surface when immersed in DMEM, both in the presence and the absence of bone marrow stromal cells. The top activity of alkaline phosphatase was also observed in such composites. It indicated a higher level of osteoblast differentiation [12]. In [15], the effect of adding Bioglass 45S5 to biphasic calcium phosphate (HA: β -TCP = 6:4) was demonstrated. It was found that composite ceramic frameworks showed the best complex characteristics at 30 wt.% Bioglass 45S5 when the phase composition consisted of the main $\text{Na}_3\text{Ca}_6(\text{PO}_4)_5$ phase and the secondary CaSiO_3 phase. Scaffolds rapidly formed an apatite layer (in 1 day), improved degradability (three times) and demonstrated good biocompatibility by cell proliferation and adhesion assays.

A minor amount of CaSiO_3 phase was developed after heat treatment at 1100 °C for 2 h. Bioceramics based on pseudowollastonite β - CaSiO_3 have good osteoconductivity and bioactivity, which was confirmed by both in vitro [42–45] and in vivo [46–48] tests. It is noted in [49] that such ceramics have good cytocompatibility and osteoblast-like cell attachment and promote better ALP activity of cells compared to controls. Plus, pseudowollastonite also possesses good bone inductivity properties, stimulates the formation of new bone on the surface and possesses a much faster resorption rate and bone formation rate compared to porous β -TCP.

Since the ceramics presented in this paper consisted of biocompatible phases investigated in the literature, it can be expected that the obtained ceramics based on TCP and SS_{aq} will show a positive trend in biocompatibility and osteoconductivity in both in vitro and in vivo tests.

Micrographs of the ceramics obtained from preceramic samples based on TCP and SS_{aq} after heat treatment at various temperatures are presented in Figure 9.

Based on the SEM data, the morphology of the ceramic samples after heat treatment differed from the morphology of preceramic samples (Figure 4b). Irregularly shaped sintered agglomerates sizes of 0.5–4.5 μm were observed at 500 °C and consisted of particles 200–400 nm in size. The grain size gradually rose during subsequent heat treatments, and by 1100 °C, the average grain size was 2.5–6.5 μm . Sintering was observed in all samples. At 500 °C, one can see “fibers” that presumably belong to the SiO_2 phase formed from the melt during cooling. The presence of such “fibers” in ceramic at upper temperatures is also not excluded, so their placement probably is local.

The similarity of morphologies (Figure 9), as well as the XRD data of the ceramics (Figure 8), can explain the similarity of the apparent density of the ceramic samples and the behavior of the volume shrinkage (Figure 10). The rise in temperature from 500 °C to 700 °C led to an increase in the apparent density of the samples from 1.44 g/cm^3 to 1.5 g/cm^3 . Perhaps this can be attributed to the formation of the β - NaCaPO_4 phase, with its likely maximum content at 700 °C. Since a further rise in temperature to 1100 °C following Figure 8 led to a chemical interaction between β - NaCaPO_4 and β - $\text{Ca}_3(\text{PO}_4)_2$ with the formation of the $\text{Na}_3\text{Ca}_6(\text{PO}_4)_5$ phase, this agreed with the data of [18]. The apparent density of the samples at 1100 °C was 1.46 g/cm^3 . A small difference in density may be due to the similarity of crystalline density: β - $\text{Ca}_3(\text{PO}_4)_2$ (3.07 g/cm^3) [50], β - NaCaPO_4 (3.12 g/cm^3) [51], $\text{Na}_3\text{Ca}_6(\text{PO}_4)_5$ (3.04 g/cm^3) [20]. The β - CaSiO_3 phase formed at 1100 °C was minor and probably did not add a significant value to the amount of apparent density.

On the other hand, it was a challenge to estimate the effect of the SiO₂ phase on the density of the ceramic samples from the data set presented in the current work.

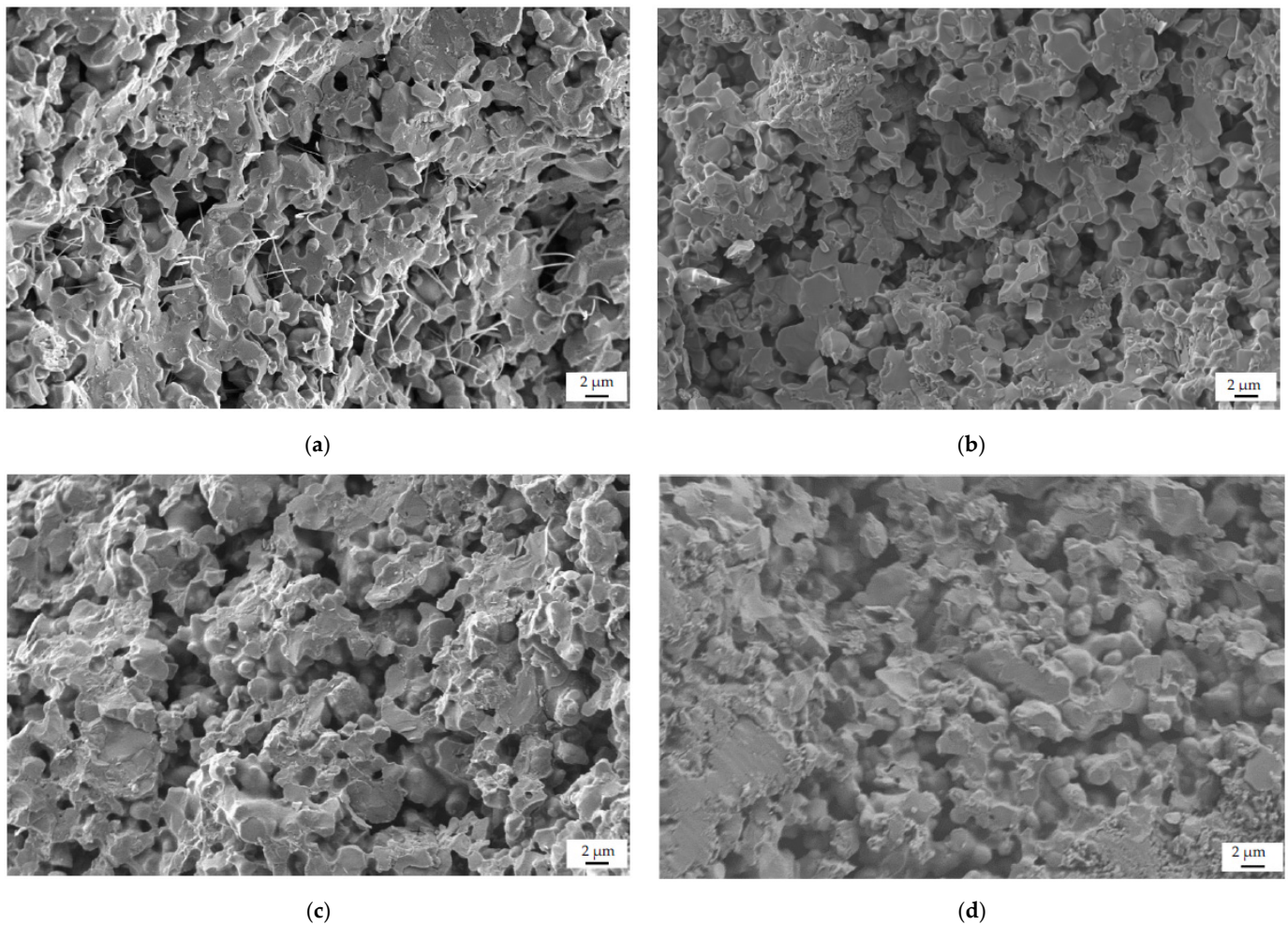


Figure 9. SEM micrographs of the ceramics after heat treatment at 500 °C (a), 700 °C (b), 900 °C (c) and 1100 °C (d).

A negative volumetric shrinkage was observed in all ceramic samples, reflecting the expansion of the ceramics as a result of the heat treatment. This effect may be related to the removal of water. At elevated temperatures, a glass based on hydrated sodium silicate was formed (Figure 7) that melted and interacted with the filler (TCP) to develop new phases. The fixation of particles (grains) may be observed at the points of contact, which also prevents shrinkage and a rise in the material density. At the same time, the viscosity of such a melt may be assessed as high. Hence, when water was removed up to ≈ 500 °C, the compositions expanded with subsequent shape retention upon cooling. Nevertheless, the expansion of the samples did not exceed 4% and decreased to $\approx 3.6\%$ with further increasing temperature to 1100 °C, which may be due to the “settling down” of the ceramics as a result of sintering.

Figure 11 shows the ceramic bending and compressive strength after firing at different temperatures. The rise of both bending and compressive resistance with increasing temperature may be related to the phase composition of the samples. Thus, when the β -NaCaPO₄ phase formed at 500 °C and 700 °C, the bending strength of the β -NaCaPO₄/ β -Ca₃(PO₄)₂ composites did not exceed 7.5 MPa. The compressive strength for those composites did not exceed 32.5 MPa. When the Na₃Ca₆(PO₄)₅ phase formed, the bending resistance of the samples increased to ≈ 9.5 MPa (900 °C) and ≈ 10.6 MPa (1100 °C), and the compressive strength increased to ≈ 42.7 MPa (900 °C) and ≈ 43.5 MPa (1100 °C). It is possible that the

strengthening effect was also achieved due to the presence of a combination of several phases and the existence of strong interfacial boundaries.

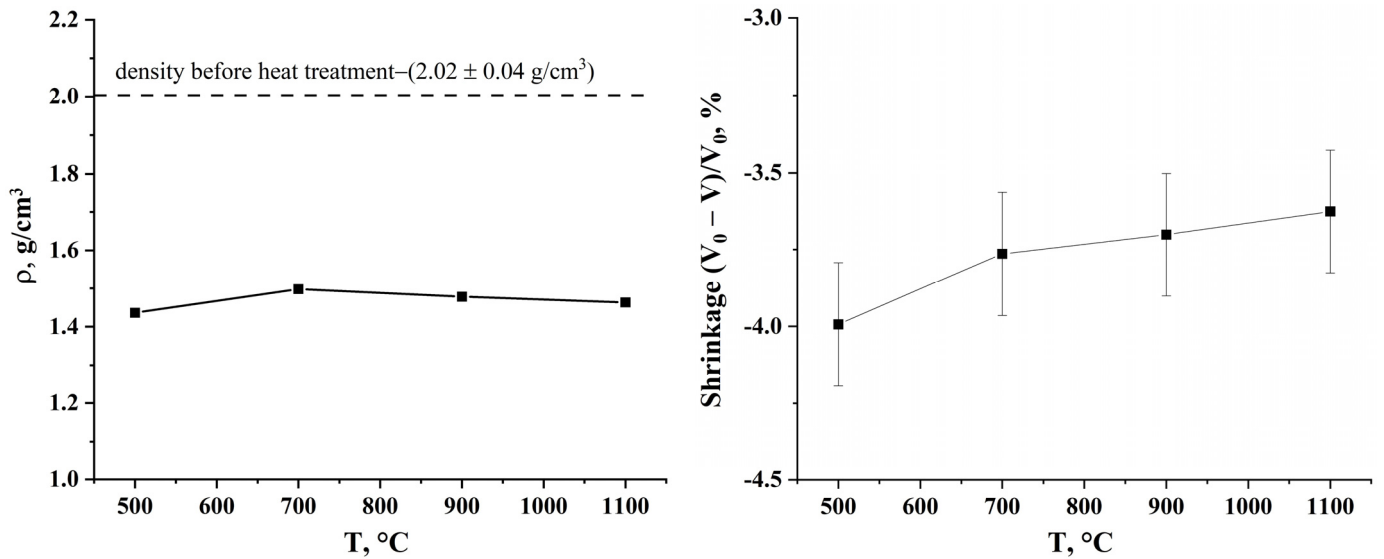


Figure 10. Apparent density (g/cm^3) and Volume shrinkage ($V_0 - V/V_0, \%$) of ceramic samples based on the tricalcium phosphate powder $\text{Ca}_3(\text{PO}_4)_2$ and the aqueous solution of sodium silicate $(\text{Na}_2\text{O} \cdot 2,87\text{SiO}_2)_{\text{aq}}$ after heat treatment at 500 °C, 700 °C, 900 °C and 1100 °C.

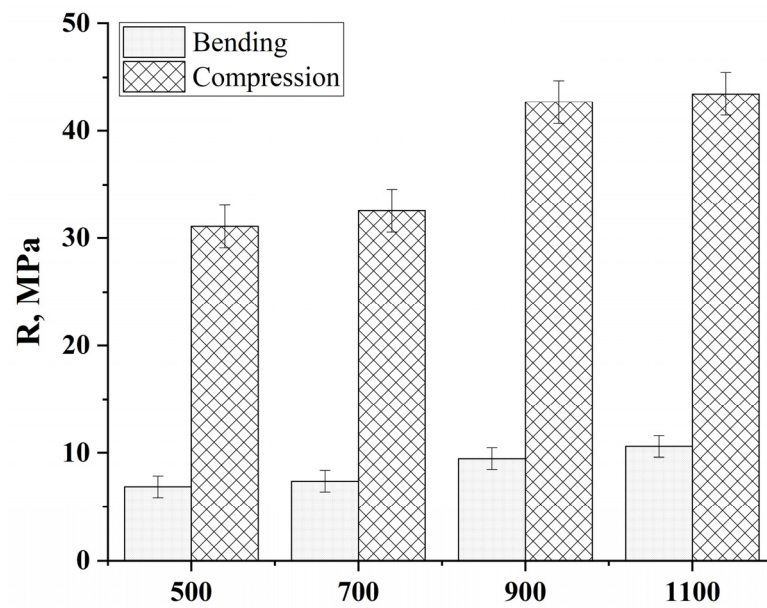


Figure 11. Bending and compressive strength of the ceramics after heat treatment at 500 °C, 700 °C, 900 °C and 1100 °C.

The work [12] demonstrated the effect of the Bioglass 45S5 additive on the phase composition of ceramic materials and their compressive strength. Sintering was carried out at 1200 °C for 4 h at a heating rate of 4 °C/min. The authors indicated that for composites of hydroxyapatite–Bioglass 45S5 (1, 2.5 and 5 wt.%), the phase composition was represented by HAP and TCP, and the compressive strength was 26, 34 and 79 MPa, respectively. However, at values of 25 wt.% Bioglass 45S5, the phase composition presented a $\text{Na}_3\text{Ca}_6(\text{PO}_4)_5$ + amorphous silicate phase. The compressive strength of such a composite increased significantly and amounted to 131 MPa. A similar trend was observed in [15] for composites of biphasic calcium phosphate (BCP)–Bioglass 45S5 with different contents

of the latter. In [16], the authors indicated that for the composites of cuttlefish powders and 30wt.% Bioglass 45S5, the phase composition was represented by HA, β -TCP and $\text{Na}_3\text{Ca}_6(\text{PO}_4)_5$ after heat treatment at 900 °C for 3 h. The compressive strength of such a material was ≈ 12.5 MPa. The compressive and bending resistance of sintered β -TCP was 83 and 21 MPa, respectively [52]. In [22], it was established that the compressive strength of the material, the composition of which was represented by β -NaCaPO₄ ss and α -cristobalite, was 54.66 MPa.

All that can indirectly confirm the assumption that the strength increases with the development of the phase combination development obtained in this work, as all ceramic samples were obtained under the same conditions and the difference was observed only in the firing temperature. Besides the phase composition of the material, it is important to note that volume shrinkage decreases with the rise of temperature to 1100 °C, so compact, dense internal structures are formed, which also contribute to the development of the ceramics' strength.

On the other hand, the XRD data (Figure 8) showed a rise in the SiO₂ phase with increasing temperature. The micrograph of the ceramic at 500 °C also illustrated "fibers" that could hypothetically refer to the SiO₂. Their local spread probably could lead to material reinforcement, increasing, in turn, the bending and compressive strength of the ceramics; however, this question remains open.

4. Conclusions

The presented research showed the possibility of using pastes based on tricalcium phosphate and an aqueous solution of sodium silicate as an extrusion material. The dependence of the plastic strength of these pastes on both time and temperature was studied. It was established that the highest plastic strength, corresponding to the fully hardened state, was achieved after 45 min at 100 °C and was $R_{100\text{ °C}} \approx 0.2$ MPa. The phase composition of ceramic was represented by unreacted β -TCP (β -Ca₃(PO₄)₂) and β -rhenanite (β -NaCaPO₄) after a heat treatment at 500 °C of preceramic samples based on tricalcium phosphate and an aqueous solution of sodium silicate. Further, an increase in temperature up to 700 °C led to the appearing phase of silicon dioxide (SiO₂) and up to 900 °C, of sodium calcium phosphate ($\text{Na}_3\text{Ca}_6(\text{PO}_4)_5$). After the heat treatment at 1100 °C, ceramics consisted of β -TCP (β -Ca₃(PO₄)₂), sodium calcium phosphate ($\text{Na}_3\text{Ca}_6(\text{PO}_4)_5$), silicon dioxide (SiO₂) and β -wollastonite (β -CaSiO₃). The apparent density of the ceramic samples was in the range of 1.44–1.5 g/cm³, with a maximum of 1.5 g/cm³ at 700 °C, corresponding to the phase composition of β -TCP (β -Ca₃(PO₄)₂), β -rhenanite (β -NaCaPO₄) and silicon dioxide (SiO₂). A negative volumetric shrinkage was observed in all samples, not exceeding 4%. The bending strength of the ceramics increased with increasing temperature from ≈ 6.8 MPa at 500 °C to ≈ 10.6 MPa at 1100 °C, and the compressive strength increased from ≈ 31.1 MPa at 500 °C to ≈ 43.5 MPa at 1100 °C. The obtained composite ceramics consisted of biocompatible phases that are widely explored in the literature. Therefore, such composites may be used as a biomaterial for the treatment of bone tissue defects.

Author Contributions: Conceptualization, M.K.; methodology, M.K.; investigation, M.K., T.S. (Tatiana Safronova), T.S. (Tatiana Shatalova), Y.F., I.T. and Y.L.; writing—original draft preparation, M.K.; writing—review and editing, M.K.; visualization, M.K., T.S. (Tatiana Safronova), T.S. (Tatiana Shatalova), Y.F., I.T. and Y.L.; supervision, T.S. (Tatiana Safronova); project administration, T.S. (Tatiana Safronova); funding acquisition, T.S. (Tatiana Safronova). All authors have read and agreed to the published version of the manuscript.

Funding: This work was carried out with financial support from the Russian Foundation for Basic Research (RFBR) (grants No. 20-03-00550 A).

Institutional Review Board Statement: Not applicable.

Data Availability Statement: Not applicable.

Acknowledgments: The research was carried out using the equipment of MSU Shared Research Equipment Center “Technologies for obtaining new nanostructured materials and their complex study” and purchased by MSU within the framework of the Equipment Renovation Program (National Project “Science”) and the MSU Program of Development.

Conflicts of Interest: The authors declare no conflict of interest.

References

- Bellucci, D.; Sola, A.; Cannillo, V. Hydroxyapatite and Tricalcium Phosphate Composites with Bioactive Glass as Second Phase: State of the Art and Current Applications. *J. Biomed. Mater. Res. A* **2016**, *104*, 1030–1056. [[CrossRef](#)] [[PubMed](#)]
- Arango-Ospina, M.; Boccaccini, A.R. Bioactive Glasses and Ceramics for Tissue Engineering. In *Tissue Engineering Using Ceramics and Polymers*; Woodhead Publishing: Sawston, UK, 2022; pp. 111–178. [[CrossRef](#)]
- Reza Rezaie, H.; Beigi Rizi, H.; Rezaei Khamseh, M.M.; Öchsner, A. A Review on Dental Materials. In *Advanced Structured Materials*; Springer International Publishing: Cham, Switzerland, 2020; Volume 123, ISBN 978-3-030-48930-4.
- Svetskaya, N.V.; Lukina, Y.S.; Larionov, D.S.; Andreev, D.V.; Sivkov, S.P. 3D-Matrix Based on Bioactive Glass and Calcium Phosphates with Controllable Resorption Rate for Bone Tissue Replacement. *Glass Ceram.* **2017**, *73*, 342–347. [[CrossRef](#)]
- Safronova, T.V.; Putlyaev, V.I.; Shekhirev, M.A.; Kuznetsov, A.V. Composite Ceramic Containing a Bioresorbable Phase. *Glass Ceram.* **2007**, *64*, 102–106. [[CrossRef](#)]
- Balamurugan, A.; El Mabrouk, K.; Pina, S.; Bousmina, M.M.; Ferreira, J.M.F. Melt-Derived Condensed Polymorphic Calcium Phosphate as Bone Substitute Material: An In Vitro Study. *J. Am. Ceram. Soc.* **2011**, *94*, 3023–3029. [[CrossRef](#)]
- Jalota, S.; Bhaduri, S.B.; Tas, A.C. A New Rhenanite (β -NaCaPO₄) and Hydroxyapatite Biphasic Biomaterial for Skeletal Repair. *J. Biomed. Mater. Res. B Appl. Biomater.* **2007**, *80B*, 304–316. [[CrossRef](#)] [[PubMed](#)]
- Bose, S.; Ke, D.; Sahasrabudhe, H.; Bandyopadhyay, A. Additive Manufacturing of Biomaterials. *Prog. Mater. Sci.* **2018**, *93*, 45–111. [[CrossRef](#)] [[PubMed](#)]
- Safronova, T.V.; Putlyaev, V.I.; Filippov, Y.Y.; Shatalova, T.B.; Naberezhnyi, D.O.; Nasriddinov, A.F.; Larionov, D.S. Ceramics Based on Powder Mixtures Containing Calcium Hydrogen Phosphates and Sodium Salts (Na₂CO₃, Na₄P₂O₇, and NaPO₃). *Inorg. Mater.* **2018**, *54*, 724–735. [[CrossRef](#)]
- Safronova, T.V.; Putlyaev, V.I.; Knotko, A.V.; Filippov, Y.Y.; Klimashina, E.S.; Ryzhov, A.P.; Saidzhonov, B.M. Powder Mixtures Based on Calcium Hydroxyapatite and Sodium Salts. *Inorg. Mater. Appl. Res.* **2018**, *9*, 726–731. [[CrossRef](#)]
- Safronova, T.V. Inorganic Materials for Regenerative Medicine. *Inorg. Mater.* **2021**, *57*, 443–474. [[CrossRef](#)]
- Demirkiran, H.; Mohandas, A.; Dohi, M.; Fuentes, A.; Nguyen, K.; Aswath, P. Bioactivity and Mineralization of Hydroxyapatite with Bioglass as Sintering Aid and Bioceramics with Na₃Ca₆(PO₄)₅ and Ca₅(PO₄)₂SiO₄ in a Silicate Matrix. *Mater. Sci. Eng. C* **2010**, *30*, 263–272. [[CrossRef](#)]
- Afonko, A.A.; Kirillova, S.A.; Almjashv, V.I. Ceramic and Composite Nanomaterials Based on Calcium Orthophosphates. *Nanosyst. Phys. Chem. Math.* **2012**, *3*, 84–102.
- Bergmann, C.; Lindner, M.; Zhang, W.; Koczur, K.; Kirsten, A.; Telle, R.; Fischer, H. 3D Printing of Bone Substitute Implants Using Calcium Phosphate and Bioactive Glasses. *J. Eur. Ceram. Soc.* **2010**, *30*, 2563–2567. [[CrossRef](#)]
- Su, J.; Hua, S.; Chen, A.; Chen, P.; Yang, L.; Yuan, X.; Qi, D.; Zhu, H.; Yan, C.; Xiao, J.; et al. Three-Dimensional Printing of Gyroid-Structured Composite Bioceramic Scaffolds with Tuneable Degradability. *Biomater. Adv.* **2022**, *133*, 112595. [[CrossRef](#)]
- Cozza, N.; Monte, F.; Bonani, W.; Aswath, P.; Motta, A.; Migliaresi, C. Bioactivity and Mineralization of Natural Hydroxyapatite from Cuttlefish Bone and Bioglass® Co-Sintered Bioceramics. *J. Tissue. Eng. Regen. Med.* **2018**, *12*, e1131–e1142. [[CrossRef](#)]
- Ando, J. Phase Diagrams of Ca₃(PO₄)₂-Mg₃(PO₄)₂ and Ca₃(PO₄)₂-CaNaPO₄ Systems. *Bull. Chem. Soc. Jpn.* **1958**, *31*, 201–205. [[CrossRef](#)]
- Han, Y.C.; Wang, X.Y.; Li, S.P. Change of Phase Composition and Morphology of Sonochemically Synthesised Hydroxyapatite Nanoparticles with Glycosaminoglycans during Thermal Treatment. *Adv. Appl. Ceram.* **2009**, *108*, 400–405. [[CrossRef](#)]
- Doi, Y.; Shimizu, Y.; Moriwaki, Y.; Aga, M.; Iwanaga, H.; Shibutani, T.; Yamamoto, K.; Iwayama, Y. Development of a New Calcium Phosphate Cement That Contains Sodium Calcium Phosphate. *Biomaterials* **2001**, *22*, 847–854. [[CrossRef](#)]
- Cousin, O.; Rivenet, M.; Boivin, J.C.; Abraham, F. A Refractory Bonding Phase Fundamental Study In The Na₂O-CaO-P₂O₅-SiO₂ System. *Phosphorus Res. Bull.* **1999**, *10*, 183–188. [[CrossRef](#)]
- El-Ghannam, A.R. Advanced Bioceramic Composite for Bone Tissue Engineering: Design Principles and Structure–Bioactivity Relationship. *J. Biomed. Mater. Res. A* **2004**, *69A*, 490–501. [[CrossRef](#)]
- Gupta, G.; El-Ghannam, A.; Kirakodu, S.; Khraisheh, M.; Zbib, H. Enhancement of Osteoblast Gene Expression by Mechanically Compatible Porous Si-Rich Nanocomposite. *J. Biomed. Mater. Res. B Appl. Biomater.* **2007**, *81B*, 387–396. [[CrossRef](#)]
- Jones, J.R. Review of Bioactive Glass: From Hench to Hybrids. *Acta Biomater.* **2013**, *9*, 4457–4486. [[CrossRef](#)] [[PubMed](#)]
- No, Y.; Li, J.; Zreiqat, H. Doped Calcium Silicate Ceramics: A New Class of Candidates for Synthetic Bone Substitutes. *Materials* **2017**, *10*, 153. [[CrossRef](#)]
- Zuev, D.M.; Klimashina, E.S.; Evdokimov, P.v.; Filippov, Y.Y.; Putlyaev, V.I. Preparation of β -Ca₃(PO₄)₂/Poly(D,L-Lactide) and β -Ca₃(PO₄)₂/Poly(ϵ -Caprolactone) Biocomposite Implants for Bone Substitution. *Inorg. Mater.* **2018**, *54*, 87–95. [[CrossRef](#)]

26. Roohani-Esfahani, S.I.; Newman, P.; Zreiqat, H. Design and Fabrication of 3D Printed Scaffolds with a Mechanical Strength Comparable to Cortical Bone to Repair Large Bone Defects. *Sci. Rep.* **2016**, *6*, srep19468. [CrossRef] [PubMed]
27. Lu, X.; Lee, Y.; Yang, S.; Hao, Y.; Evans, J.R.G.; Parini, C.G. Solvent-Based Paste Extrusion Solid Freeforming. *J. Eur. Ceram. Soc.* **2010**, *30*, 1–10. [CrossRef]
28. Fu, Q.; Saiz, E.; Tomsia, A.P. Direct Ink Writing of Highly Porous and Strong Glass Scaffolds for Load-Bearing Bone Defects Repair and Regeneration. *Acta Biomater.* **2011**, *7*, 3547–3554. [CrossRef]
29. Al-Qutaifi, S.; Nazari, A.; Bagheri, A. Mechanical Properties of Layered Geopolymer Structures Applicable in Concrete 3D-Printing. *Constr. Build. Mater.* **2018**, *176*, 690–699. [CrossRef]
30. Takadama, H.; Kim, H.M.; Kokubo, T.; Nakamura, T. Mechanism of Biom mineralization of Apatite on a Sodium Silicate Glass: TEM–EDX Study In Vitro. *Chem. Mater.* **2001**, *13*, 1108–1113. [CrossRef]
31. Golovanova, O.A.; Zaits, A.V. Biomimetic Coating of a Titanium Substrate with Silicon-Substituted Hydroxyapatite. *Inorg. Mater.* **2018**, *54*, 1124–1130. [CrossRef]
32. Kaimonov, M.; Safronova, T.; Shatalova, T.; Filippov, Y.; Tikhomirova, I.; Sergeev, N. Composite Ceramics in the Na₂O–CaO–SiO₂–P₂O₅ System Obtained from Pastes Including Hydroxyapatite and an Aqueous Solution of Sodium Silicate. *Ceramics* **2022**, *5*, 550–561. [CrossRef]
33. ICDD. PDF-4+ 2010 (Database); Kabekkodu, S., Ed.; International Centre for Diffraction Data: Newtown Square, PA, USA, 2010. Available online: <https://www.icdd.com/pdf-2/> (accessed on 15 July 2022).
34. Korneev, V.I.; Danilov, V.V. *Soluble and Liquid Glass*; Stroy-izdat: St. Petersburg, Russia, 1996.
35. Greaves, G.N.; Sen, S. Inorganic Glasses, Glass-Forming Liquids and Amorphizing Solids. *Adv. Phys.* **2007**, *56*, 1–166. [CrossRef]
36. Yashima, M.; Sakai, A.; Kamiyama, T.; Hoshikawa, A. Crystal Structure Analysis of β -Tricalcium Phosphate Ca₃(PO₄)₂ by Neutron Powder Diffraction. *J. Solid State Chem.* **2003**, *175*, 272–277. [CrossRef]
37. Morozov, V.A.; Belik, A.A.; Kotov, R.N.; Presnyakov, I.A.; Khasanov, S.S.; Lazoryak, B.I. Crystal Structures of Double Calcium and Alkali Metal Phosphates Ca₁₀M(PO₄)₇(M = Li, Na, K). *Crystallogr. Rep.* **2000**, *45*, 13–20. [CrossRef]
38. Catauro, M.; Bollino, F.; Papale, F. Synthesis of SiO₂ System via Sol–Gel Process: Biocompatibility Tests with a Fibroblast Strain and Release Kinetics. *J. Biomed. Mater. Res. A* **2014**, *102*, 1677–1680. [CrossRef]
39. Catauro, M.; Bollino, F.; Papale, F.; Gallicchio, M.; Pacifico, S. Influence of the Polymer Amount on Bioactivity and Biocompatibility of SiO₂/PEG Hybrid Materials Synthesized by Sol–Gel Technique. *Mater. Sci. Eng. C* **2015**, *48*, 548–555. [CrossRef]
40. Vapirov, V.V.; Feoktistov, V.M.; Venskovich, A.A.; Vapirova, N.V. On Silicon’s Behavior and Its Biological Role In Nature. *Sci. Notes Petrozavodsk. State Univ.* **2017**, *2*, 95–102.
41. Ahmad, H. Biocompatible SiO₂ in the Fabrication of Stimuli-Responsive Hybrid Composites and Their Application Potential. *J. Chem.* **2015**, *2015*, 846328. [CrossRef]
42. Zhang, N.; Molenda, J.A.; Fournelle, J.H.; Murphy, W.L.; Sahai, N. Effects of Pseudowollastonite (CaSiO₃) Bioceramic on in Vitro Activity of Human Mesenchymal Stem Cells. *Biomaterials* **2010**, *31*, 7653–7665. [CrossRef]
43. Sarmiento, C.; Luklinska, Z.B.; Brown, L.; Anseau, M.; de Aza, P.N.; de Aza, S.; Hughes, F.J.; McKay, I.J. In Vitro Behavior of Osteoblastic Cells Cultured in the Presence of Pseudowollastonite Ceramic. *J. Biomed. Mater. Res. A* **2004**, *69A*, 351–358. [CrossRef]
44. Sahai, N.; Anseau, M. Cyclic Silicate Active Site and Stereochemical Match for Apatite Nucleation on Pseudowollastonite Bioceramic–Bone Interfaces. *Biomaterials* **2005**, *26*, 5763–5770. [CrossRef]
45. Ni, S.; Chang, J.; Chou, L.; Zhai, W. Comparison of Osteoblast-like Cell Responses to Calcium Silicate and Tricalcium Phosphate Ceramics in Vitro. *Wiley Online Libr.* **2006**, *80*, 174–183. [CrossRef]
46. de Aza, P.N.; Luklinska, Z.B.; Martinez, A.; Anseau, M.R.; Guitian, F.; de Aza, S.; de Aza, S. Morphological and Structural Study of Pseudowollastonite Implants in Bone. *J. Microsc.* **2000**, *197*, 60–67. [CrossRef]
47. Xue, W.; Liu, X.; Zheng, X.; Ding, C. In Vivo Evaluation of Plasma-Sprayed Wollastonite Coating. *Biomaterials* **2005**, *26*, 3455–3460. [CrossRef] [PubMed]
48. Xu, S.; Lin, K.; Wang, Z.; Chang, J.; Wang, L.; Lu, J.; Ning, C. Reconstruction of Calvarial Defect of Rabbits Using Porous Calcium Silicate Bioactive Ceramics. *Biomaterials* **2008**, *29*, 2588–2596. [CrossRef]
49. Srinath, P.; Abdul Azeem, P.; Venugopal Reddy, K. Review on Calcium Silicate-Based Bioceramics in Bone Tissue Engineering. *Int. J. Appl. Ceram. Technol.* **2020**, *17*, 2450–2464. [CrossRef]
50. Dickens, B.; Schroeder, L.W.; Brown, W.E. Crystallographic Studies of the Role of Mg as a Stabilizing Impurity in β -Ca₃(PO₄)₂. The Crystal Structure of Pure β -Ca₃(PO₄)₂. *J. Solid State Chem.* **1974**, *10*, 232–248. [CrossRef]
51. ben Amara, M.; Vlasse, M.; le Flem, G.; Hagenmuller, P. Structure of the Low-Temperature Variety of Calcium Sodium Orthophosphate, NaCaPO₄. *Acta Cryst. C* **1983**, *39*, 1483–1485. [CrossRef]
52. Liu, X.; Ei-Ghannam, A. Effect of Processing Parameters on the Microstructure and Mechanical Behavior of Silica–Calcium Phosphate Nanocomposite. *J. Mater. Sci. Mater. Med.* **2010**, *21*, 2087–2094. [CrossRef]